

Article

Rational Design, Synthesis and Preliminary Evaluation of Novel Fusarinine C-Based Chelators for Radiolabeling with Zirconium-89

Chuangyan Zhai ^{1,2}, Shanzhen He ³, Yunjie Ye ³, Christine Rangger ², Piriya Kaeopookum ², Dominik Summer ², Hubertus Haas ⁴, Leopold Kremser ⁵, Herbert Lindner ⁵, Julie Foster ⁶, Jane Sosabowski ⁶ and Clemens Decristoforo ^{2,*}

¹ School of Forensic Medicine, Southern Medical University, 510515 Guangzhou, China; zhaichuangyan@smu.edu.cn

² Department of Nuclear Medicine, Medical University Innsbruck, 6020 Innsbruck, Austria; christine.rangger@i-med.ac.at (C.R.); gamsuk@hotmail.com (P.K.); Dominik.summer@i-med.ac.at (D.S.)

³ Department of Nuclear Medicine, Guangdong Academy of Medical Sciences, 510080 Guangzhou, China; candido.he@163.com (S.H.); gdsy1970@163.com (Y.Y.)

⁴ Division of Molecular Biology, Biocenter, Medical University Innsbruck, 6020 Innsbruck, Austria; Hubertus.Haas@i-med.ac.at

⁵ Division of Clinical Biochemistry, Biocenter, Medical University of Innsbruck, 6020 Innsbruck, Austria; Leopold.Kremser@i-med.ac.at (L.K.); Herbert.Lindner@i-med.ac.at (H.L.)

⁶ Centre for Molecular Oncology, Barts Cancer Institute, Queen Mary University of London, E1 4NS London, UK; j.m.foster@qmul.ac.uk (J.F.); j.k.sosabowski@qmul.ac.uk (J.S.)

* Correspondence: Clemens.Decristoforo@i-med.ac.at; Tel.: +43-512-504-80951; Fax: +43-512-504-6780951

Received: 23 November 2018; Accepted: 25 February 2019; Published: 6 March 2019



Abstract: Fusarinine C (FSC) has recently been shown to be a promising and novel chelator for ⁸⁹Zr. Here, FSC has been further derivatized to optimize the complexation properties of FSC-based chelators for ⁸⁹Zr-labeling by introducing additional carboxylic groups. These were expected to improve the stability of ⁸⁹Zr-complexes by saturating the 8-coordination sphere of [⁸⁹Zr] Zr⁴⁺, and also to introduce functionalities suitable for conjugation to targeting vectors such as monoclonal antibodies. For proof of concept, succinic acid derivatization at the amine groups of FSC was carried out, resulting in FSC(succ)₂ and FSC(succ)₃. FSC(succ)₂ was further derivatized to FSC(succ)₂ AA by reacting with acetic anhydride (AA). The Zr⁴⁺ complexation properties of these chelators were studied by reacting with ZrCl₄. Partition coefficient, protein binding, serum stability, acid dissociation, and transchelation studies of ⁸⁹Zr-complexes were carried out in vitro and the results were compared with those for ⁸⁹Zr-desferrioxamine B ([⁸⁹Zr]Zr-DFO) and ⁸⁹Zr-triacetylfusarinine C ([⁸⁹Zr]Zr-TAFC). The in vivo properties of [⁸⁹Zr]Zr-FSC(succ)₃ were further compared with [⁸⁹Zr]Zr-TAFC in BALB/c mice using micro-positron emission tomography/computer tomography (microPET/CT) imaging. Fusarinine C (succ)₂AA and FSC(succ)₃ were synthesized with satisfactory yields. Complexation with ZrCl₄ was achieved using a simple strategy resulting in high-purity Zr-FSC(succ)₂AA and Zr-FSC(succ)₃ with 1:1 stoichiometry. Distribution coefficients of ⁸⁹Zr-complexes revealed increased hydrophilic character compared to [⁸⁹Zr]Zr-TAFC. All radioligands showed high stability in phosphate buffered saline (PBS) and human serum and low protein-bound activity over a period of seven days. Acid dissociation and transchelation studies exhibited a range of in vitro stabilities following the order: [⁸⁹Zr]Zr-FSC(succ)₃ > [⁸⁹Zr]Zr-TAFC > [⁸⁹Zr]Zr-FSC(succ)₂AA >> [⁸⁹Zr]Zr-DFO. Biodistribution studies of [⁸⁹Zr]Zr-FSC(succ)₃ revealed a slower excretion pattern compared to [⁸⁹Zr]Zr-TAFC. In conclusion, [⁸⁹Zr]Zr-FSC(succ)₃ showed the best stability and inertness. The promising results obtained with [⁸⁹Zr]Zr-FSC(succ)₂AA highlight the potential of FSC(succ)₂ as a monovalent chelator for conjugation to targeted biomolecules, in particular, monoclonal antibodies.

Keywords: fusarinine C (FSC); zirconium-89; bifunctional chelator; immuno-positron emission tomography (PET)

1. Introduction

Immuno-positron emission tomography (PET) is of great value for the development of monoclonal antibodies (mAbs) as therapeutic targeting vectors, enabling tracking and quantification of radiolabeled mAbs at high resolution and sensitivity [1]. In recent years, Zirconium-89 (^{89}Zr), in particular, has become the most commonly-studied positron-emitting radionuclide for immuno-PET imaging. The physical half-life of 78.4 h is a good match with the biological half-life of mAbs, thus increasing the utility of PET in the development of this class of compound, and its medium mean positron energy of 0.395 MeV allows high-resolution PET imaging [2]. Additionally, in contrast to iodine-124, another long-lived positron-emitter, which has a rapid release of radioiodine from the cell after internalization, ^{89}Zr is a residualizing radiometal and facilitates the visualization of tumors [3]. As an osteophilic radionuclide, immuno-PET imaging with ^{89}Zr requires stable coordination of the radionuclide with the chelator to minimize dissociation resulting in bone accumulation in vivo.

To date, desferrioxamine B (DFO), see Figure 1, has been the most widely used bifunctional chelating system for ^{89}Zr -based radiopharmaceuticals. Although chelation with DFO results in complexes with acceptable stability in pre-clinical as well as some clinical studies, it is far from being optimal due to the partial release of $[\text{}^{89}\text{Zr}]\text{Zr}^{4+}$ from the chelating system [4]. The released $[\text{}^{89}\text{Zr}]\text{Zr}^{4+}$ has been reported to accumulate in bone, particularly at late time points (3–7 days), which results in a decrease in image contrast, as well as an increase in radiation dose, especially to bone marrow [5–10]. The instability of DFO is attributed to the linear structure (which allows easy access to challenging cations and natural chelators in vivo), as well as to the incomplete saturation of the 8-coordination sphere of Zr^{4+} [11]. The development of novel high-stability Zr^{4+} -ligands to minimize the uptake of liberated Zr^{4+} in the bone and other non-targeted tissue is an interesting and important goal. While many investigators focus on the optimization of the conjugation moiety between DFO and the biomolecule, attempts to develop new chelators are increasing [12–22]. Several novel octadentate and oxygen-rich ^{89}Zr -chelators have been reported showing improved in vitro stability. These novel chelators are designed to be acyclic or macrocyclic by the addition of another hydroxamate unit [12,13,17,19,21] or introduce new chelating groups such as hydroxypyridinone and pyrocatechol groups [14–16,20].

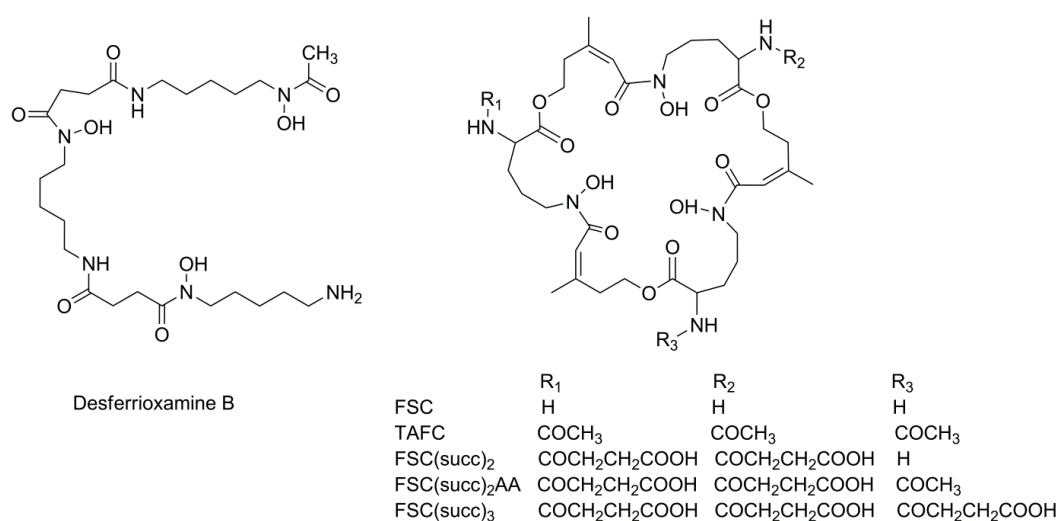


Figure 1. Structures of desferrioxamine B (DFO), fusarinine C (FSC), triacetylfusarinine C (TAFC), FSC(succ)₂, FSC(succ)₂AA and FSC(succ)₃.

Recently, we reported that fusarinine C (FSC), which has a 36-membered ring structure and three bidentate hydroxamates to coordinate ^{89}Zr , showed superior stability and kinetic inertness compared to DFO. In particular, the excellent targeting properties of FSC bioconjugates in PET-imaging studies showed FSC to be a highly promising alternative chelator for ^{89}Zr [23–25]. However, since FSC is hexadentate rather than octadentate, we postulated that improvements could be expected by introducing additional coordinating groups to saturate the coordination sphere of $[\text{}^{89}\text{Zr}]\text{Zr}^{4+}$. Another potential drawback of FSC as a ^{89}Zr -bifunctional chelator lies in it having three functionalities for derivatization, which, despite facilitating the employment of multivalent concepts for small molecules, are not suitable for conjugation to macromolecules, especially antibodies. Therefore, a further aim of this study was to design a FSC-based mono-functional ^{89}Zr -chelator. As proof of concept, modifications via succinic acid derivatization resulting in FSC(succ)₂ acetic anhydride (AA) and FSC(succ)₃, see Figure 1, were developed. This straightforward modification introduces additional carboxylic acid groups known to coordinate with Zr, which additionally can be utilized for bioconjugation strategies. In this study, the in vitro stability and transchelation properties of these ^{89}Zr -complexes were investigated and compared with $[\text{}^{89}\text{Zr}]\text{Zr}$ -DFO and ^{89}Zr -triacetylfusarinine C ($[\text{}^{89}\text{Zr}]\text{Zr}$ -TAFC). The in vivo properties of $[\text{}^{89}\text{Zr}]\text{Zr}$ -FSC(succ)₃ were further compared with $[\text{}^{89}\text{Zr}]\text{Zr}$ -TAFC in BALB/c mice.

2. Materials and Methods

All commercially available reagents were of reagent grade and used as supplied with no further purification. Desferrioxamine B was obtained from Genaxxon Bioscience GmbH (Ulm, Germany). Triacetylfusarinine C was prepared and purified as described previously [23]. $[\text{}^{89}\text{Zr}]\text{Zr}$ -oxalate was purchased from Perkin Elmer, Inc (Waltham, MA, US) with an activity concentration of 900–1000 MBq per milliliter.

Purification of compounds was performed via a preparative reversed-phase high-performance liquid chromatography system (preparative RP-HPLC) using a Gilson 322 HPLC pump, a Gilson ultraviolet (UV)/VIS-155 detector (Gilson International B.V., Limburg, Germany), and a Eurosil Bioselect Vertex Plus 300 × 8 mm 5 μm C_{18A} 300 Å column (Knauer, Berlin, Germany) with a flow rate of 3.0 mL/min. The gradient was as follows: 0–1.0 min 10% acetonitrile (CH₃CN), 1.0–18.0 min 10–40% CH₃CN (gradient A).

Analytical RP-HPLC analysis was performed with an UltiMate 3000 RS HPLC pump, an UltiMate 3000 RS column compartment (column oven temperature was set at 25 °C), an UltiMate 3000 UV-Vis variable wavelength detector (Dionex, Gemering, Germany), and a Raytest radiometric detector (Raytest GmbH, Straubenhardt, Germany). A Vydac 218 TP5215, 150 × 3.0 mm column (SRD, Vienna, Austria), flow rate 1.0 mL/min, and UV-Vis detection at 220/410 nm were employed with the following CH₃CN/H₂O/0.1% trifluoroacetic acid (TFA) gradient: 0–0.5 min 0% CH₃CN/0.1% TFA, 0.5–7.0 min, 0–55% CH₃CN/0.1% TFA (gradient B).

2.1. Fusarinine C

Fusarinine C was produced as described previously [23]. Briefly, the *Aspergillus fumigatus* mutant strain ΔsidG was cultured in iron-free minimal medium with 1% glucose for 36 h at 37 °C and 200 rpm. Biomass was removed by filtration. The media-containing siderophore was collected and concentrated. Additional purification was performed via preparative RP-HPLC (gradient A, $t_{\text{R}} = 10.2$ min) followed by concentration and lyophilization. Analytical RP-HPLC (gradient B): $t_{\text{R}} = 4.7$ min.

2.2. Fusarinine C (succ)₃

To FSC (50 mg, 69 μmol) dissolved in 1 mL dimethylformamide (DMF), 34.5 mg of succinic anhydride (5 eq, 0.34 mmol) was added and the pH was adjusted to 4.5 using *N,N*-diisopropylethylamine (DIPEA). After shaking for 0.5 h, FSC(succ)₃ was directly isolated via preparative RP-HPLC (gradient A, $t_{\text{R}} = 12.1$ min) and confirmed by matrix-assisted laser desorption/ionization time of flight mass spectrometry (MALDI-TOF-MS). The collected fractions

were concentrated and lyophilized. FSC(succ)₃: yield: 63 mg, (61 μmol), 88%; MALDI TOF-MS: [M + H]⁺ = 1028.2 [C₄₅H₆₆N₆O₂₁; exact mass: 1026.4 (calculated)]. Analytical RP-HPLC (gradient B): t_R = 5.6 min.

2.3. Fusarinine C(succ)₂

The general synthesis procedure of FSC(succ)₂ was the same as that of FSC(succ)₃ except that a 2 eq molar excess of succinic anhydride was used. FSC(succ)₂ was isolated from the byproducts (FSC-succ and FSC(succ)₃) via preparative RP-HPLC (gradient A, t_R = 11.5 min). FSC(succ)₂: yield: 28 mg, (30 μmol), 43%. MALDI TOF-MS: [M + H]⁺ = 928.2 [C₄₁H₆₂N₆O₁₈; exact mass: 926.4 (calculated)]. Analytical RP-HPLC (gradient B): t_R = 5.4 min.

2.4. Fusarinine C(succ)₂AA

To FSC(succ)₂ (10 mg, 11 μmol) dissolved in 0.5 mL DMF, 1 mL of acetic anhydride (AA) was added. After shaking for 10 min, FSC(succ)₂AA was quickly isolated via preparative RP-HPLC (gradient A, t_R = 11.9 min) and confirmed by MALDI-TOF-MS. The collected fractions were concentrated and lyophilized. FSC(succ)₂AA: yield: 9 mg, (9.3 μmol), 85%. MALDI TOF-MS: [M + H]⁺ = 970.1 [C₄₃H₆₄N₆O₁₉; exact mass: 968.4 (calculated)]. Analytical RP-HPLC (gradient B): t_R = 5.6 min.

2.5. Zr-Fusarinine C(succ)₂AA and Zr-Fusarinine C(succ)₃.

ZrCl₄ (121 mg) was dissolved in 1 mL 0.1 M hydrochloric acid solution resulting in a concentration of 0.52 M. After dissolving FSC(succ)₂AA (5 mg, 5.2 μmol) or FSC(succ)₃ (5 mg, 4.9 μmol) in 1 mL water, a 1.2 eq molar excess of ZrCl₄ (11.9 μL and 11.3 μL, respectively) was added. The reaction solutions were shaken gently for 5 min, then loaded onto a pre-activated Sep-Pak C₁₈ cartridge. After washing the cartridge with 10 mL water, Zr-FSC(succ)₂AA and Zr-FSC(succ)₃ were eluted with 1 mL methanol. The eluate fractions were dried by evaporation under nitrogen and weighed. The identities of the products were confirmed by electrospray ionization mass spectrometry (ESI-MS). Zr-FSC(succ)₂AA: yield: 3.6 mg, (3.4 μmol), 65%. ESI-MS: [M + H]⁺ = 1,055.3 [C₄₃H₆₀N₆O₁₉Zr, see Figure 2A; exact mass: 1054.3 (calculated)]. RP-HPLC (gradient B): t_R = 5.4 min. Zr-FSC(succ)₃: yield: 3.7 mg, (3.3 μmol), 67%. ESI-MS: [M + H]⁺ = 1113.3 [C₄₅H₆₂N₆O₂₁Zr, see Figure 2B; exact mass: 1112.3 (calculated)]. Analytical RP-HPLC (gradient B): t_R = 5.3 min.

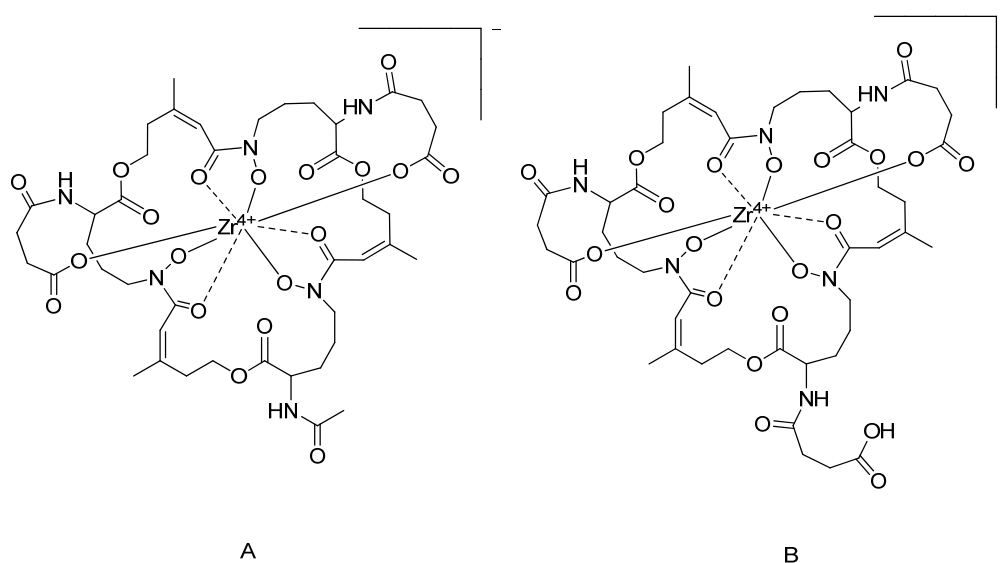


Figure 2. Postulated coordination structures of Zr-FSC(succ)₂AA (A) and Zr-FSC(succ)₃ (B).

2.6. ^{89}Zr -Labeling

Approximately 30 MBq (30 μL) of ^{89}Zr]Zr-oxalate was mixed with 27 μL of sodium carbonate (Na_2CO_3 , 1 M) and incubated for 3 min at room temperature (RT) [26]. Thereafter, 100 μL of 4-(2-hydroxyethyl)-1-piperazineethanesulfonic acid (HEPES) buffer (0.5 M, pH 7.0) was added to the reaction vial. Either DFO (32.8 μg), TAFC (42.6 μg), FSC(succ) $_2$ AA (48.5 μg) or FSC(succ) $_3$ (51.4 μg) was added to the reaction vial. The labeling mixture was allowed to react at RT with a pH between 6.8 and 7.2 for 90 min. The reaction progress was monitored via analytical RP-HPLC (gradient B): ^{89}Zr]Zr-DFO: $t_R = 4.8$ min, ^{89}Zr]Zr-TAFC: $t_R = 5.9$ min, ^{89}Zr]Zr-FSC(succ) $_2$ AA: $t_R = 6.1$ min, and ^{89}Zr]Zr-FSC(succ) $_3$: $t_R = 6.0$ min.

For animal experiments, 60 μL of CaCl_2 (0.5 M) was added to the radiolabeling solution and a precipitate of Ca-oxalate appeared. The solution was then passed through a 0.2- μm filter to remove Ca-oxalate which may cause kidney failure. Subsequently, the filtrate was diluted to an appropriate volume using saline for administration to the BALB/c mice.

2.7. In Vitro Characterization

2.7.1. Distribution Coefficient

A volume of 500 μL PBS including 0.5 MBq radioligand (^{89}Zr]Zr-FSC(succ) $_2$ AA or ^{89}Zr]Zr-FSC(succ) $_3$) was combined with 500 μL octanol. The mixture was vortexed for 15 min, and centrifuged for 2 min at 2000 rcf. Subsequently, 50 μL aliquots of the aqueous and the octanol layer were collected, measured in a 2480 Wizard² Automatic Gamma Counter (Perkin Elmer, Vienna, Austria), and distribution coefficient (logD) values were calculated using Excel 2013 ($n = 5$) (Redmond, WA, USA).

2.7.2. Stability Assay

Determination of the stability of ^{89}Zr]Zr-DFO, ^{89}Zr]Zr-TAFC, ^{89}Zr]Zr-FSC(succ) $_2$ AA and ^{89}Zr]Zr-FSC(succ) $_3$ was carried out by incubating the radioligands in PBS, a 1000-fold molar excess of ethylenediaminetetraacetic acid (EDTA) solution (radioligand vs. EDTA: 25 μM vs. 25 mM) with different pH (pH 7, pH 6, and pH 4), as well as in human serum (the human serum was obtained from author C.D. with his consent at the Medical University Innsbruck within a routine blood withdrawal procedure) for seven days at 37 $^\circ\text{C}$. At selected time points, PBS and EDTA samples were analyzed in triplicate directly via analytical RP-HPLC, while serum aliquots were mixed with 500 μL of CH_3CN , vortexed, and centrifuged at 20,000 rcf for 2 min. Then, the precipitate was washed three times using CH_3CN before analysis.

2.7.3. Transchelation Study

^{89}Zr]Zr-DFO (50 μL) was mixed with a 1000-fold molar excess of either FSC(succ) $_2$ AA or FSC(succ) $_3$ and ^{89}Zr]Zr-TAFC (or ^{89}Zr]Zr-FSC(succ) $_2$ AA, ^{89}Zr]Zr-FSC(succ) $_3$) (50 μL each) was mixed with a 1000-fold molar excess of DFO and incubated for seven days at RT. At selected time points, aliquots of the solutions were analyzed in triplicate directly via analytical RP-HPLC. The transchelation was determined by the ratio of ^{89}Zr]Zr-DFO and ^{89}Zr]Zr-FSC derivatives.

2.7.4. Protein Binding Assay

The protein binding property was evaluated by incubating ^{89}Zr]Zr-FSC(succ) $_2$ AA or ^{89}Zr]Zr-FSC(succ) $_3$ for seven days at 37 $^\circ\text{C}$ in fresh human serum. Subsequently, 30 μL of the solution was passed through a size exclusion spin column (MicroSpinG-50 column, GE Healthcare, Buckinghamshire, UK) via centrifugation at 2000 rcf for 2 min. Protein binding of the complexes in triplicate was determined by measuring the activity on the column (non-protein bound) and the activity in the eluate (protein bound) in the gamma counter.

2.7.5. Biodistribution Study

All animal experiments were conducted in compliance with the Austrian animal protection laws and with the approval of the Austrian Ministry of Science (BMWF-66.011/0049-WF/II/3b/2014) or were approved by the Animal Welfare and Ethical Review Body at Queen Mary University of London, and the UK Home Office (Project Licence 70/7603).

For the evaluation of biodistribution, four female BALB/c mice (Charles River Laboratories, Sulzfeld, Germany) were intravenously injected with [⁸⁹Zr]Zr-FSC(succ)₃ (1.5 MBq/mouse, 4.8 µg precursor) or [⁸⁹Zr]Zr-TAFC (1.5 MBq/mouse, 4 µg) into the tail vein and sacrificed by cervical dislocation at 6 h post injection (p.i.). Organs (spleen, pancreas, stomach, intestine, kidney, liver, heart, and lung), blood, muscle tissue, and bone were dissected, weighed and then measured in the gamma counter to calculate the percentage of injected dose per gram of tissue (% ID/g). Statistical analysis was performed using an independent two-population *t*-test (significance level *p* = 0.05) and Origin 6.1 software (Northampton, MA, USA).

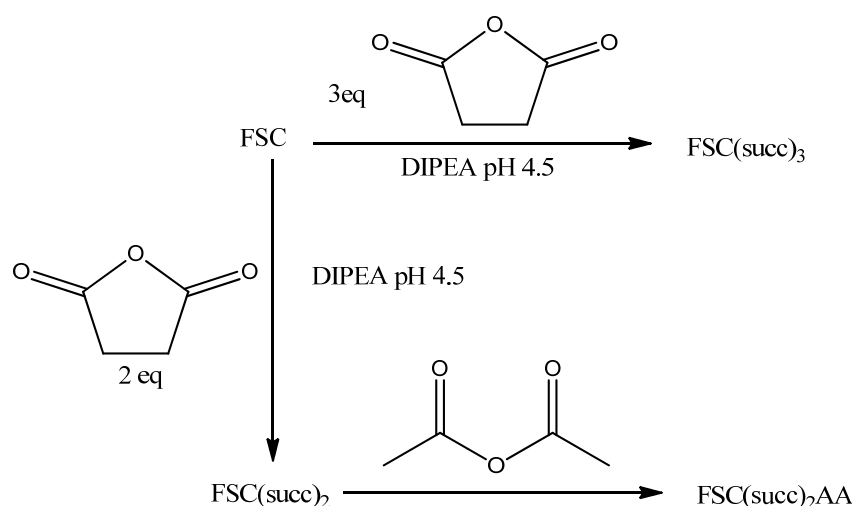
2.7.6. Micro-Positron Emission Tomography/Computer Tomography Imaging

Micro-Positron Emission Tomography/computer tomography (MicroPET/CT) imaging studies were carried out using an Inveon microPET/CT scanner (Siemens Preclinical Solutions, Knoxville, TN, USA). Healthy female BALB/c mice were injected intravenously with 5 MBq of either [⁸⁹Zr]Zr-FSC(succ)₃ (16 µg, *n* = 1) or [⁸⁹Zr]Zr-TAFC (13 µg, *n* = 1). MicroPET/CT images were acquired under general anesthesia (isoflurane/O₂) for 20 min. Imaging data were recorded via static scans at 80 min and 24 h p.i. The microPET/CT scans were reconstructed and merged with OSEM3D-SPMAP (PET, matrix size 256 × 256) and Feldkamp (CT, Shepp Logan filter). For evaluation of bone uptake, image-based quantitation was carried out by selecting volumes of interest around each knee region and % ID/cm³ were calculated for both time points (VivoQuant image analysis software, Invivo LLC, Boston, MA, USA) and expressed as mean values of left and right knees to compare both compounds.

3. Results

3.1. Synthesis

The straightforward synthesis of FSC(succ)₂AA and FSC(succ)₃ is shown in Scheme 1. Fusarinine C was reacted with succinic anhydride at pH 4.5 resulting in FSC(succ)₃ and FSC(succ)₂ in satisfactory yields of 88 ± 4.0% and 43 ± 4.5%, respectively. The unreacted amine group of FSC(succ)₂ was further derivatized with a molar excess of acetic anhydride resulting in the final compound FSC(succ)₂AA. High-performance liquid chromatograms demonstrated the purity of compounds above 96%, see Supplementary Materials, Figures S1–S3. Zr-FSC(succ)₂AA and Zr-FSC(succ)₃ were produced by the complexation of precursors with a molar excess of ZrCl₄ in 0.1 M HCl solution at pH 1 within 5 min. Reaction of excess of precursor with ZrCl₄ (0.1 eq) showed a comparable reaction efficiency. ESI-MS demonstrated not only the metal-to-ligand ratio of 1:1 but also the high-purity of Zr-complexes by analyzing the distinctive isotopic ratios of zirconium, see Supplementary Materials, Figures S4–S6.



Scheme 1. Synthesis strategies of FSC(succ)₃ and FSC(succ)₂AA.

3.2. ⁸⁹Zr-Labeling

The ⁸⁹Zr-labeling procedure of DFO, TAFC, FSC(succ)₂AA and FSC(succ)₃ was as previously described [23]. Quantitative radiolabeling was achieved in HEPES buffer at RT between pH 6.8 to 7.2 within 90 min. Quality control was carried out by analytical RP-HPLC (instead of the instant thin-layer chromatography (ITLC) method for [⁸⁹Zr]Zr-DFO and [⁸⁹Zr]Zr-TAFC reported previously in which [⁸⁹Zr]Zr-DFO and [⁸⁹Zr]Zr-TAFC remain at the origin and free [⁸⁹Zr]Zr⁴⁺ migrates with the solvent front). This change was due to the undesirable spread of [⁸⁹Zr]Zr-FSC(succ)₂AA and [⁸⁹Zr]Zr-FSC(succ)₃ along the ITLC strips.

3.3. Ex Vitro Characterization

Fusarinine C(succ)₂AA and FSC(succ)₃ showed high solubility in water, which is comparable to TAFC but different from recently reported novel octadentate chelators which seem to have poor solubility [9]. The lower logD values of [⁸⁹Zr]Zr-FSC(succ)₂AA and [⁸⁹Zr]Zr-FSC(succ)₃ (-3.3 ± 0.1 and -3.5 ± 0.4 , respectively) indicate higher hydrophilic properties than [⁸⁹Zr]Zr-DFO and [⁸⁹Zr]Zr-TAFC (-3.0 ± 0.1 and -2.0 ± 0.0 , respectively). All radioligands showed high stability in PBS and human serum over a period of seven days and no demetallation was observed. The low protein-bound activity (<10%) over the whole monitoring period further confirmed the stability of radioligands in human serum. The logD, protein binding and stability in human serum data for [⁸⁹Zr]Zr-FSC(succ)₂AA and [⁸⁹Zr]Zr-FSC(succ)₃ are summarized in Table 1 and compared with previously reported data of [⁸⁹Zr]Zr-DFO and [⁸⁹Zr]Zr-TAFC [23].

Table 1. LogD, protein binding, and stability in human data for [⁸⁹Zr]Zr-DFO, [⁸⁹Zr]Zr-TAFC, [⁸⁹Zr]Zr-FSC(succ)₂AA and [⁸⁹Zr]Zr-FSC(succ)₃.

⁸⁹ Zr-Complex	Log D	Incubation Time (days)	Protein Binding (%)	Stability in Human Serum (%)
[⁸⁹ Zr]Zr-DFO	-3.0 ± 0.1	7	8.7 ± 1.0	99.3
[⁸⁹ Zr]Zr-TAFC	-2.0 ± 0.0	7	6.8 ± 0.5	99.5
[⁸⁹ Zr]Zr-FSC(succ) ₂ AA	-3.3 ± 0.1	7	5.9 ± 1.6	99.4
[⁸⁹ Zr]Zr-FSC(succ) ₃	-3.5 ± 0.4	7	8.3 ± 3.5	99.5

Acid dissociation experiments and transchelation studies were performed to compare the relative kinetic inertness of [⁸⁹Zr]Zr-DFO, [⁸⁹Zr]Zr-TAFC, [⁸⁹Zr]Zr-FSC(succ)₂AA and [⁸⁹Zr]Zr-FSC(succ)₃. Data of dissociation experiments are summarized in Figure 3. Briefly, at pH 7, [⁸⁹Zr]Zr-TAFC, [⁸⁹Zr]Zr-FSC(succ)₂AA and [⁸⁹Zr]Zr-FSC(succ)₃ revealed excellent resistance to transchelation over

seven days, in contrast to that for $[^{89}\text{Zr}]\text{Zr-DFO}$ where almost 60% transchelation occurred, see Figure 3A. At pH 6, $[^{89}\text{Zr}]\text{Zr-FSC}(\text{succ})_3$ remained intact (97.8%), being more stable than $[^{89}\text{Zr}]\text{Zr-TAFC}$ (94.4%) and significantly higher than $[^{89}\text{Zr}]\text{Zr-FSC}(\text{succ})_2\text{AA}$ (76%), see Figure 3B. At pH 4, the difference in stability of $[^{89}\text{Zr}]\text{Zr-FSC}(\text{succ})_3$ and $[^{89}\text{Zr}]\text{Zr-TAFC}$ was more pronounced (87.9 vs. 70.3% of intact complex, respectively, at day 7), see Figure 3C.

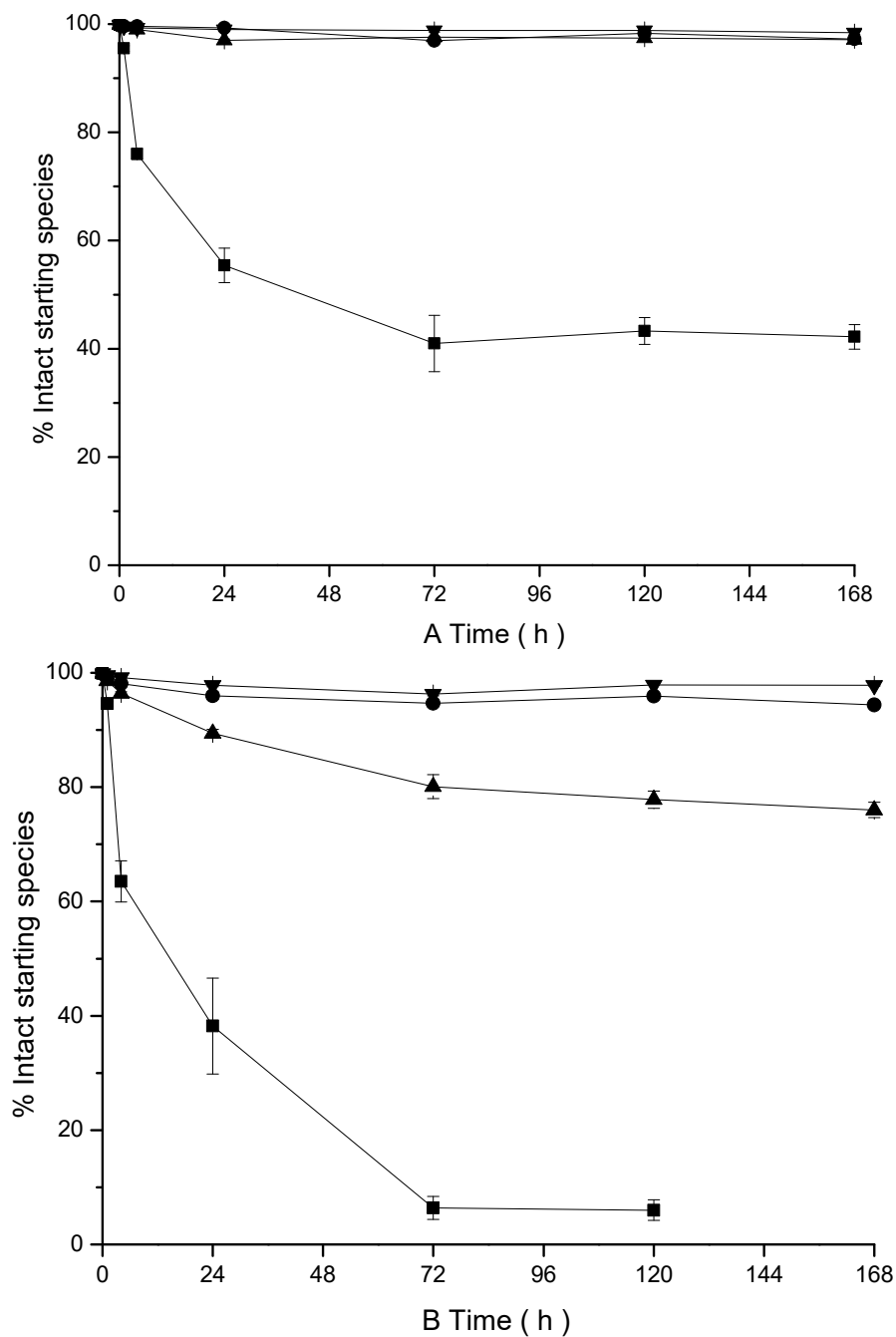


Figure 3. Cont.

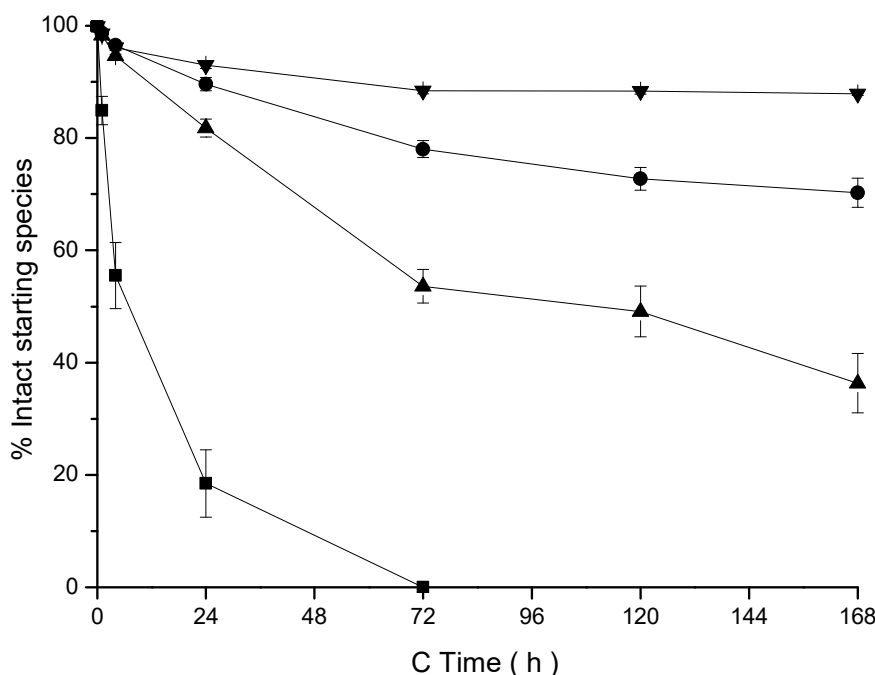


Figure 3. Acid dissociation studies of [⁸⁹Zr]Zr-DFO (■), [⁸⁹Zr]Zr-TAFC (●), [⁸⁹Zr]Zr-FSC(succ)₂AA (▲) and [⁸⁹Zr]Zr-FSC(succ)₃ (▼) in a 1000-fold molar excess of EDTA solution at pH 7 (A), pH 6 (B), and pH 4 (C).

Transchelation experiments are shown in Figure 4 and were performed by incubating: (A) [⁸⁹Zr]Zr-DFO in a 1000-fold molar excess of FSC(succ)₂AA or FSC(succ)₃, or (B) [⁸⁹Zr]Zr-TAFC, [⁸⁹Zr]Zr-FSC(succ)₂AA and [⁸⁹Zr]Zr-FSC(succ)₃ incubated in a 1000-fold molar excess of DFO. The transchelation ratio of (A) ⁸⁹Zr from [⁸⁹Zr]Zr-DFO to FSC(succ)₂AA and FSC(succ)₃ or (B) from [⁸⁹Zr]Zr-TAFC, [⁸⁹Zr]Zr-FSC(succ)₂AA and [⁸⁹Zr]Zr-FSC(succ)₃ to DFO was easily calculated due to the significant difference of the retention time of radioligands. Almost quantitative transchelation of ⁸⁹Zr from [⁸⁹Zr]Zr-DFO to FSC(succ)₂AA or FSC(succ)₃ was observed within 1 h. In contrast, [⁸⁹Zr]Zr-TAFC, [⁸⁹Zr]Zr-FSC(succ)₂AA and [⁸⁹Zr]Zr-FSC(succ)₃ showed a stronger resistance to transchelation to DFO. After 7 days, [⁸⁹Zr]Zr-FSC(succ)₃ showed the highest kinetic inertness (62.1% of intact complex) compared with [⁸⁹Zr]Zr-TAFC and [⁸⁹Zr]Zr-FSC(succ)₂AA (39.8% and 30.8% of intact complex, respectively).

3.4. Biodistribution Study and Micro-Positron Emission Tomography/Computer Tomography (microPET/CT) Imaging

Based on the above-mentioned results, [⁸⁹Zr]Zr-FSC(succ)₃ and [⁸⁹Zr]Zr-TAFC were further compared in vivo. Biodistribution data of [⁸⁹Zr]Zr-FSC(succ)₃ and [⁸⁹Zr]Zr-TAFC are presented in Figure 5. Both radioligands show rapid clearance from the body, mainly through the kidneys and a rather low uptake, especially, in bones. A relatively slower blood clearance for [⁸⁹Zr]Zr-FSC(succ)₃ than for [⁸⁹Zr]Zr-TAFC was observed (0.11 ± 0.08 vs. $0.05 \pm 0.01\%$ ID/g). Correspondingly, activity in heart ($0.28 \pm 0.08\%$ ID/g), lung ($0.21 \pm 0.04\%$ ID/g), muscle ($0.25 \pm 0.07\%$ ID/g), and bone ($0.24 \pm 0.04\%$ ID/g) were also higher. The microPET/CT images of the BALB/c mouse at 80 min p.i. and 24 h p.i. injected with either [⁸⁹Zr]Zr-FSC(succ)₃ or [⁸⁹Zr]Zr-TAFC further confirmed similar rapid pharmacokinetics, see Figure 6, three-dimensional images: Supplementary Materials, Figures S7–S10. The kidneys and bladder were the primarily visible structures, which is related to excretion and kidney retention. At 80 min p.i. [⁸⁹Zr]Zr-FSC(succ)₃ showed some gall bladder activity and some minor activity in the small bowel which disappeared in the late images. More importantly, no bone uptake was observed, confirming the high in vivo stability of both compounds. An image-based quantitative comparison of bone uptake in the knee of mice revealed an even lower uptake of [⁸⁹Zr]Zr-FSC(succ)₃

with 0.083 and 0.026% ID/cm³ and of [⁸⁹Zr]Zr-TAFC with 0.040 and 0.016% ID/cm³ at 80 min and 24 h, respectively, underlining the high in vivo stability of both chelates.

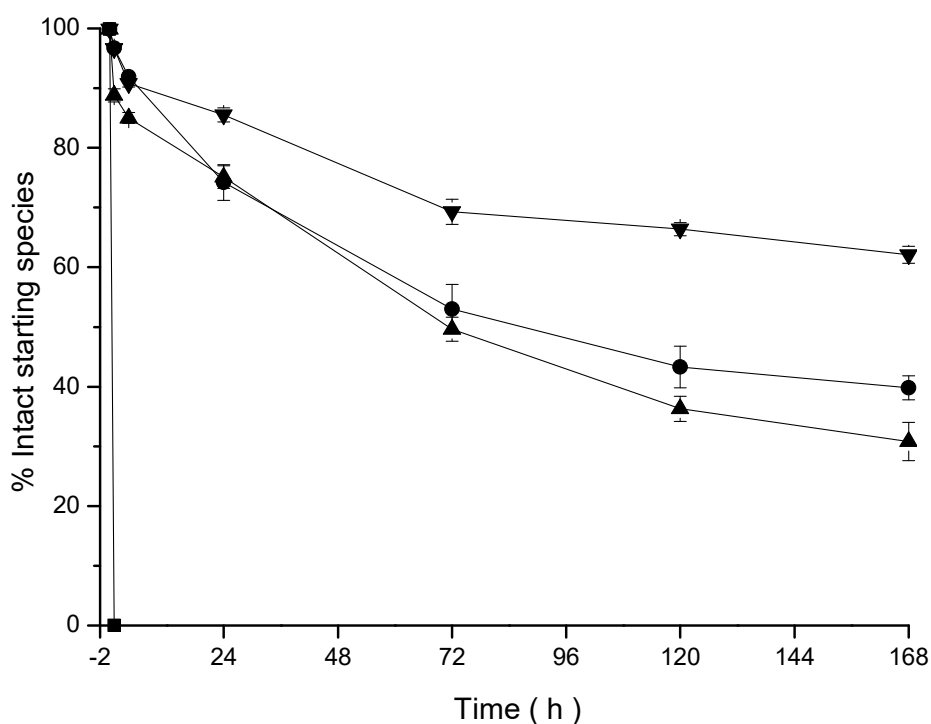


Figure 4. Transchelation studies: Percent of intact [⁸⁹Zr]Zr-DFO (—■—) incubated in a 1000-fold molar excess of FSC(succ)₃ or FSC(succ)₂AA, and [⁸⁹Zr]Zr-TAFC (—●—), [⁸⁹Zr]Zr-FSC(succ)₂AA (—▲—) and [⁸⁹Zr]Zr-FSC(succ)₃ (—▼—) incubated in a 1000-fold excess of DFO.

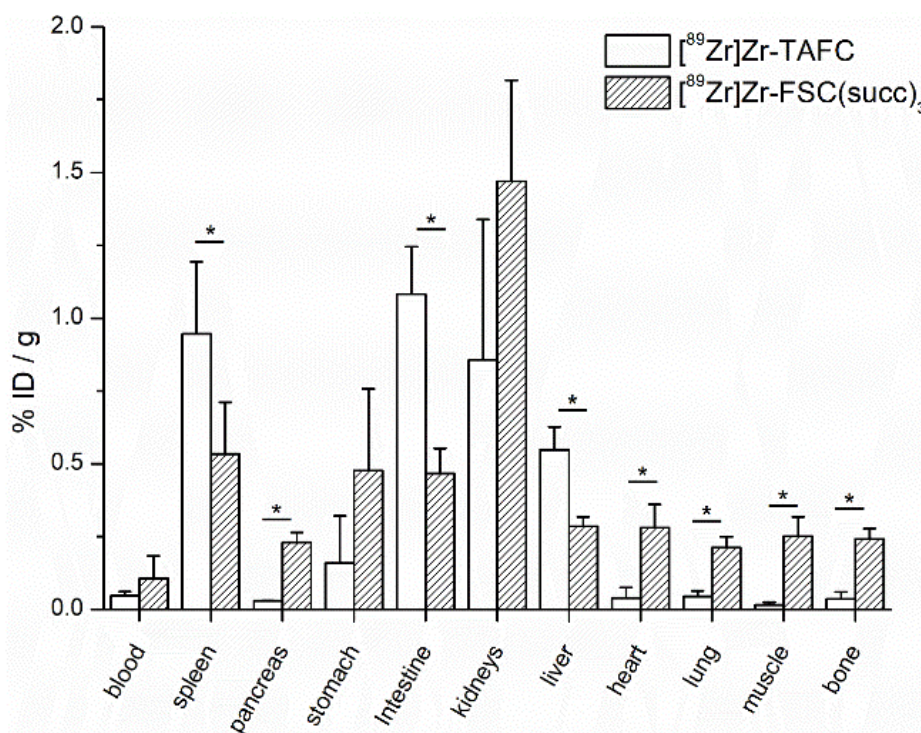


Figure 5. Comparison of biodistribution data of [⁸⁹Zr]Zr-FSC(succ)₃ (4.8 μg, 1.5 MBq, n = 4) with [⁸⁹Zr]Zr-TAFC (4 μg, 1.5 MBq, n = 4) at 6 h post infection (p.i.) in BALB/c mice. * indicates significant differences between the two compounds (p < 0.05).

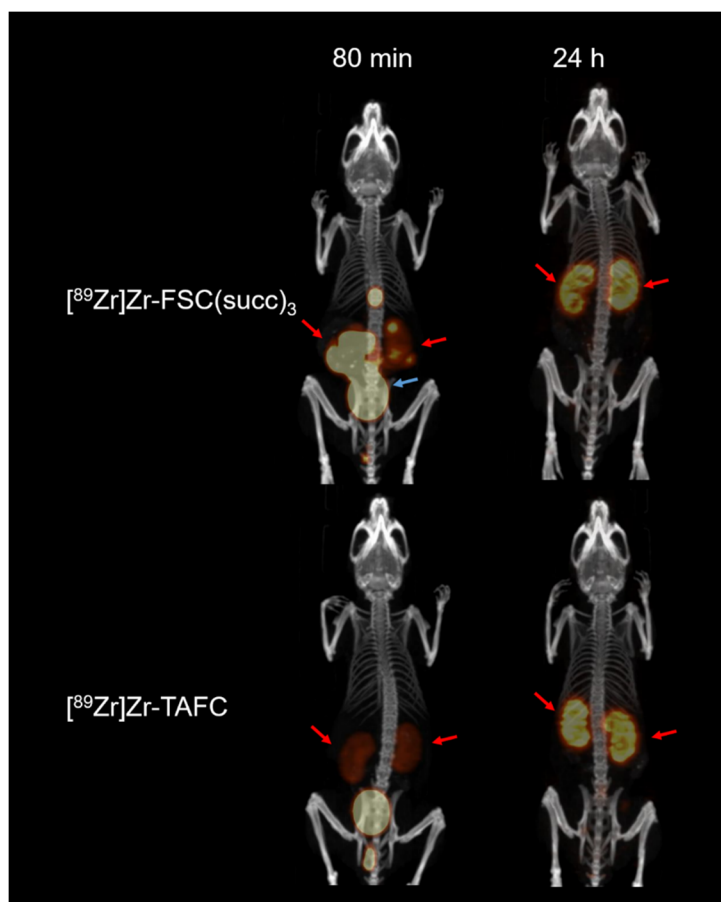


Figure 6. Micro-positron emission tomography/computer tomography images at 80 min p.i. and 24 h p.i. of BALB/c mice injected with either $[^{89}\text{Zr}]\text{Zr-FSC(succ)}_3$ or $[^{89}\text{Zr}]\text{Zr-TAFC}$. Red arrow indicator: kidneys; blue arrow indicator: bladder. The single focal accumulation in the image of $[^{89}\text{Zr}]\text{Zr-FSC(succ)}_3$ 80 min p.i. is related to gall bladder activity, additionally some activity in small bowel appears, which disappears at 24 h p.i.

4. Discussion

The high potential of FSC as a novel multivalent ^{89}Zr -bifunctional chelator was demonstrated by our group recently [23]. However, the six coordinating oxygens of FSC do not coordinatively saturate the Zr^{4+} . In addition, three of the functionalities of FSC may limit its application to the macromolecules, especially antibodies. On this basis, we were interested in designing novel chelators based on FSC by introducing two or three carboxylic functional groups, which were expected to, on one hand, improve the stability of complexation by saturating the coordination sphere of $[^{89}\text{Zr}]\text{Zr}^{4+}$ and, on the other hand, reduce the number of conjugation groups making them suitable for conjugation to mAbs.

As proof of concept, two or three succinic acid groups were introduced into the FSC skeleton and FSC(succ)_2 , $\text{FSC(succ)}_2\text{AA}$ and FSC(succ)_3 were synthesized with satisfactory yields. In our previous report, we discovered that iron protection is required for coupling FSC with targeting vectors [23]. However, the present study revealed that FSC can couple active groups such as anhydride groups at acidic pH, which provides a simpler conjugation approach. Moreover, the successful synthesis of FSC(succ)_2 and $\text{FSC(succ)}_2\text{AA}$ opens a way to apply it to mAbs. FSC(succ)_2 , which has only one free amine functionality left, possesses the potential to couple mAbs with an activated group resulting in a monomeric $\text{FSC(succ)}_2\text{-mAb}$.

In this study, the rapid and quantitative complexing of $\text{FSC(succ)}_2\text{AA}$ and FSC(succ)_3 with ZrCl_4 was reported and confirmed by ESI-MS. In our previous papers, we reported simple quantitative binding of ZrCl_4 with TAFC at acidic pH (1–5) within 5 min [23] and quantitative labeling of TAFC with

^{89}Zr -oxalate using acetate buffer [27]. On the basis of these findings, we can anticipate that $^{89}\text{Zr}[\text{ZrCl}_4]$ may be a better choice for labeling FSC derivatives in acetate buffer at appropriate pH. The advantage of $^{89}\text{Zr}[\text{ZrCl}_4]$ over ^{89}Zr -oxalate lies not only in the shorter labeling time but also in avoiding the use of highly concentrated oxalate solution which potentially can result in the production of solid calcium oxalate causing kidney damage. In contrast to HEPES buffer, which requires additional quality control before clinical application, acetate buffer is entirely pharmaceutically compatible. For better understanding the exact coordination structures as well as their influence on stability, the preparation of single crystals of Zr-TAFC, Zr-FSC(succ)₂AA and Zr-FSC(succ)₃ for X-ray Diffraction was explored using different strategies; however, this failed. Multivalent hydroxamates seem not to crystallize easily, and this may be the reason that Zr(Me-AHA)₄ is the only successfully crystallized Zr-hydroxamate compound [11].

To assess the relative kinetic inertness of $^{89}\text{Zr}[\text{Zr-DFO}]$, $^{89}\text{Zr}[\text{Zr-TAFC}]$, $^{89}\text{Zr}[\text{Zr-FSC(succ)}_2\text{AA}]$ and $^{89}\text{Zr}[\text{Zr-FSC(succ)}_3]$, acid dissociation experiments were performed under acidic conditions. At pH 4, $^{89}\text{Zr}[\text{Zr-FSC(succ)}_3]$ was the most kinetically inert compound to acid dissociation for seven days, with $^{89}\text{Zr}[\text{Zr-TAFC}]$ showing moderate stability, followed by $^{89}\text{Zr}[\text{Zr-FSC(succ)}_2\text{AA}]$, and $^{89}\text{Zr}[\text{Zr-DFO}]$ totally decomposing on day 3. Transchelation studies showed the same but more pronounced trend. $^{89}\text{Zr}[\text{Zr-DFO}]$ showed total transchelation within 1 h whereas other ^{89}Zr -complexes only showed limited transchelation after seven days. The improved stability and kinetic inertness of $^{89}\text{Zr}[\text{Zr-FSC(succ)}_3]$, $^{89}\text{Zr}[\text{Zr-TAFC}]$, and $^{89}\text{Zr}[\text{Zr-FSC(succ)}_2\text{AA}]$ over $^{89}\text{Zr}[\text{Zr-DFO}]$ were attributed to the macrocyclic structure. The superior stability of $^{89}\text{Zr}[\text{Zr-FSC(succ)}_3]$ over $^{89}\text{Zr}[\text{Zr-TAFC}]$ and $^{89}\text{Zr}[\text{Zr-FSC(succ)}_2\text{AA}]$ may be as a result of the higher coordination number and better coordination configuration. The lower stability of $^{89}\text{Zr}[\text{Zr-FSC(succ)}_2\text{AA}]$ compared to $^{89}\text{Zr}[\text{Zr-TAFC}]$ may be related to the loss of the symmetrical structure. However, the superior stability of $^{89}\text{Zr}[\text{Zr-FSC(succ)}_2\text{AA}]$ over $^{89}\text{Zr}[\text{Zr-DFO}]$ highlights the potential of FSC(succ)₂ as a monomeric chelator in the development of novel ^{89}Zr -tracers.

A direct biodistribution comparison revealed a much slower blood clearance of $^{89}\text{Zr}[\text{Zr-FSC(succ)}_3]$ than $^{89}\text{Zr}[\text{Zr-TAFC}]$, resulting in a higher uptake in all major organs. Notably, the bone activity of $^{89}\text{Zr}[\text{Zr-FSC(succ)}_3]$ was significantly higher than that of $^{89}\text{Zr}[\text{Zr-TAFC}]$, possibly mainly reflecting the slower clearance rather than being actual bone uptake. Even though different time points were chosen for an imaging study, this was confirmed by images at 24 h p.i. showing both radioligands without visible bone uptake. $^{89}\text{Zr}[\text{Zr-FSC(succ)}_3]$ also showed some hepatobiliary excretion in microPET/CT images at the early time point of 80 min, which was not depicted at 24 h p.i. and in the 6 h p.i. biodistribution study. The overall difference in biodistribution may be attributed to the difference in the chelate-radiometal net charge and polarity. $^{89}\text{Zr}[\text{Zr-TAFC}]$ possesses a positive net charge while $^{89}\text{Zr}[\text{Zr-FSC(succ)}_3]$ shows an overall negative charge character, which may potentially influence the excretion patterns of radiotracers. However, the difference in clearance rates between $^{89}\text{Zr}[\text{Zr-FSC(succ)}_3]$ and $^{89}\text{Zr}[\text{Zr-TAFC}]$ should not be a concern in its final application. Upon conjugation to a targeting biomolecule, the pharmacokinetics of the $^{89}\text{Zr}[\text{Zr-FSC(succ)}_3]$ complex will be completely superseded by those of biomacromolecules. Higher kidney and lower liver uptake compared to $^{89}\text{Zr}[\text{Zr-TAFC}]$ indicates a renal excretion pathway, which is consistent with the higher hydrophilicity of $^{89}\text{Zr}[\text{Zr-FSC(succ)}_3]$.

5. Conclusions

In our study, three FSC derivatives were synthesized and labeled with zirconium-89. $^{89}\text{Zr}[\text{Zr-FSC(succ)}_2\text{AA}]$ showed superiority over $^{89}\text{Zr}[\text{Zr-DFO}]$ in vitro. Furthermore, $^{89}\text{Zr}[\text{Zr-FSC(succ)}_3]$ revealed the best stability and inertness in comparison to $^{89}\text{Zr}[\text{Zr-DFO}]$, $^{89}\text{Zr}[\text{Zr-TAFC}]$ and $^{89}\text{Zr}[\text{Zr-FSC(succ)}_2\text{AA}]$. The superiority of FSC(succ)₃ was attributed to the higher coordination number and better coordination configuration. The successful synthesis of FSC(succ)₂ and FSC(succ)₂AA highlights the potential of FSC(succ)₂ as a monovalent ^{89}Zr -chelator for the conjugation to mAbs. Further studies of FSC(succ)₂-conjugated mAbs, especially in vivo, in comparison with their DFO counterparts

and potentially other novel Zr-chelators, are needed to show the true potential of this approach for Immuno-PET.

Supplementary Materials: The following are available online at <http://www.mdpi.com/2218-273X/9/3/91/s1>, Figure S1: HPLC chromatogram of purified FSC(succ)₂, Figure S2: HPLC chromatogram of purified FSC(succ)₂AA, Figure S3: HPLC chromatogram of purified FSC(succ)₃, Figure S4: The ESI-MS of [^{nat}Zr]FSC(succ)₃, Figure S5: The ESI-MS of [^{nat}Zr]FSC(succ)₂AA, Figure S6: The calculated isotope pattern for C₄₅H₆₃N₆O₂₁Zr ([^{nat}Zr]FSC(succ)₃), Figure S7: 3D microPET/CT images of [⁸⁹Zr]Zr-FSC(succ)₃ in a mouse 80min p.i., Figure S8: 3D microPET/CT images of [⁸⁹Zr]Zr-FSC(succ)₃ in a mouse 24h p.i., Figure S9: 3D microPET/CT images of [⁸⁹Zr]Zr-TAFC in a mouse 80min p.i., Figure S10 3D microPET/CT images of [⁸⁹Zr]Zr-TAFC in a mouse 24h p.i.

Author Contributions: Conceptualization, C.D. and C.Z.; methodology, C.Z., S.H., Y.Y., P.K., D.S., L.K. and J.F.; software, C.Z. and S.H.; validation, C.R. and Y.Y.; formal analysis, C.Z. and C.R.; investigation, C.D., C.Z., H.L. and J.S.; resources, C.D., H.H., H.L. and J.S.; data curation, C.D. and C.Z.; writing—original draft preparation, C.Z. and C.D.; writing—review and editing, C.R., and J.S.; visualization, J.F. and J.S.; supervision, C.D.; project administration, C.D.; funding acquisition, C.D., C.Z., H.H.

Funding: We acknowledge the financial support of the National Natural Science Foundation of China (NSFC) grant 81701738, Austrian Science Foundation (FWF) grants P 25899-B23, I 1346, and Natural Science Foundation of Guangdong Province (project No. 2017A030310526).

Conflicts of Interest: The authors declare that they have no conflict of interest.

References

1. Van Dongen, G.A.; Visser, G.W.; Lub-de Hooge, M.N.; De Vries, E.G.; Perk, L.R. Immuno-PET: A navigator in monoclonal antibody development and applications. *Oncologist* **2007**, *12*, 1379–1389. [[CrossRef](#)] [[PubMed](#)]
2. Fischer, G.; Seibold, U.; Schirmacher, R.; Wangler, B.; Wangler, C. ⁸⁹Zr, a radiometal nuclide with high potential for molecular imaging with PET: Chemistry, applications and remaining challenges. *Molecules* **2013**, *18*, 6469–6490. [[CrossRef](#)] [[PubMed](#)]
3. Stillebroer, A.B.; Franssen, G.M.; Mulders, P.F.; Oyen, W.J.; van Dongen, G.A.; Laverman, P.; Oosterwijk, E.; Boerman, O.C. ImmunoPET imaging of renal cell carcinoma with ¹²⁴I- and ⁸⁹Zr-labeled anti-CAIX monoclonal antibody cG250 in mice. *Cancer Biother. Radiopharm.* **2013**, *28*, 510–515. [[CrossRef](#)] [[PubMed](#)]
4. van de Watering, F.C.; Rijpkema, M.; Perk, L.; Brinkmann, U.; Oyen, W.J.; Boerman, O.C. Zirconium-89 labeled antibodies: A new tool for molecular imaging in cancer patients. *BioMed Res. Int.* **2014**, *2014*, 203601. [[CrossRef](#)] [[PubMed](#)]
5. Chang, A.J.; DeSilva, R.; Jain, S.; Lears, K.; Rogers, B.; Lapi, S. ⁸⁹Zr-radiolabeled trastuzumab imaging in orthotopic and metastatic breast tumors. *Pharmaceuticals* **2012**, *5*, 79–93. [[CrossRef](#)] [[PubMed](#)]
6. Aerts, H.J.; Dubois, L.; Perk, L.; Vermaelen, P.; van Dongen, G.A.; Wouters, B.G.; Lambin, P. Disparity between in vivo EGFR expression and ⁸⁹Zr-labeled cetuximab uptake assessed with PET. *J. Nucl. Med.* **2009**, *50*, 123–131. [[CrossRef](#)] [[PubMed](#)]
7. Holland, J.P.; Divilov, V.; Bander, N.H.; Smith-Jones, P.M.; Larson, S.M.; Lewis, J.S. ⁸⁹Zr-DFO-J591 for immunoPET of prostate-specific membrane antigen expression in vivo. *J. Nucl. Med.* **2010**, *51*, 1293–1300. [[CrossRef](#)] [[PubMed](#)]
8. Zeglis, B.M.; Mohindra, P.; Weissmann, G.I.; Divilov, V.; Hilderbrand, S.A.; Weissleder, R.; Lewis, J.S. Modular strategy for the construction of radiometalated antibodies for positron emission tomography based on inverse electron demand diels–Alder click chemistry. *Bioconjug. Chem.* **2011**, *22*, 2048–2059. [[CrossRef](#)] [[PubMed](#)]
9. van Rij, C.M.; Sharkey, R.M.; Goldenberg, D.M.; Frielink, C.; Molkenboer, J.D.; Franssen, G.M.; van Weerden, W.M.; Oyen, W.J.G.; Boerman, O.C. Imaging of prostate cancer with immuno-PET and immuno-SPECT using a radiolabeled anti-EGP-1 monoclonal antibody. *J. Nucl. Med.* **2011**, *52*, 1601–1607. [[CrossRef](#)] [[PubMed](#)]
10. Heskamp, S.; van Laarhoven, H.W.; Molkenboer-Kuenen, J.D.; Franssen, G.M.; Versleijen-Jonkers, Y.M.; Oyen, W.J.; van der Graaf, W.T.; Boerman, O.C. ImmunoSPECT and immunoPET of IGF-1R expression with the radiolabeled antibody R1507 in a triple-negative breast cancer model. *J. Nucl. Med.* **2010**, *51*, 1565–1572. [[CrossRef](#)] [[PubMed](#)]
11. Guérard, F.; Lee, Y.-S.; Tripier, R.; Szajek, L.P.; Deschamps, J.R.; Brechbiel, M.W. Investigation of Zr(IV) and ⁸⁹Zr(IV) complexation with hydroxamates: Progress towards designing a better chelator than desferrioxamine B for immuno-PET imaging. *Chem. Commun.* **2013**, *49*, 1002–1004. [[CrossRef](#)] [[PubMed](#)]

12. Patra, M.; Bauman, A.; Mari, C.; Fischer, C.A.; Blacque, O.; Häussinger, D.; Gasser, G.; Mindt, T.L. An octadentate bifunctional chelating agent for the development of stable zirconium-89 based molecular imaging probes. *Chem. Commun.* **2014**, *50*, 11523–11525. [[CrossRef](#)] [[PubMed](#)]
13. Guérard, F.; Lee, Y.S.; Brechbiel, M.W. Rational Design, Synthesis, and Evaluation of Tetrahydroxamic Acid Chelators for Stable Complexation of Zirconium (IV). *Chem. A Eur. J.* **2014**, *20*, 5584–5591. [[CrossRef](#)] [[PubMed](#)]
14. Pandya, D.N.; Pailloux, S.; Tatum, D.; Magda, D.; Wadas, T.J. Di-macrocylic terephthalamide ligands as chelators for the PET radionuclide zirconium-89. *Chem. Commun.* **2015**, *51*, 2301–2303. [[CrossRef](#)] [[PubMed](#)]
15. Ma, M.T.; Meszaros, L.K.; Paterson, B.M.; Berry, D.J.; Cooper, M.S.; Ma, Y.; Hider, R.C.; Blower, P.J. Tripodal tris(hydroxypyridinone) ligands for immunoconjugate PET imaging with $^{89}\text{Zr}^{4+}$: Comparison with desferrioxamine-B. *Dalton Trans.* **2015**, *44*, 4884–4900. [[CrossRef](#)] [[PubMed](#)]
16. Deri, M.A.; Ponnala, S.; Zeglis, B.M.; Pohl, G.; Dannenberg, J.J.; Lewis, J.S.; Francesconi, L.C. An alternative chelator for ^{89}Zr radiopharmaceuticals: Radiolabeling and evaluation of 3,4,3-(LI-1, 2-HOPO). *J. Med. Chem.* **2014**, *57*, 4849–4860. [[CrossRef](#)] [[PubMed](#)]
17. Seibold, U.; Wangler, B.; Wangler, C. Rational Design, Development, and Stability Assessment of a Macrocylic Four-Hydroxamate-Bearing Bifunctional Chelating Agent for ^{89}Zr . *ChemMedChem* **2017**, *12*, 1555–1571. [[CrossRef](#)] [[PubMed](#)]
18. Rousseau, J.; Zhang, Z.; Dias, G.M.; Zhang, C.; Colpo, N.; Benard, F.; Lin, K.S. Design, synthesis and evaluation of novel bifunctional tetrahydroxamate chelators for PET imaging of ^{89}Zr -labeled antibodies. *Bioorg. Med. Chem. Lett.* **2017**, *27*, 708–712. [[CrossRef](#)] [[PubMed](#)]
19. Boros, E.; Holland, J.P.; Kenton, N.; Robile, N.; Caravan, P. Macrocycle-Based Hydroxamate Ligands for Complexation and Immunoconjugation of $^{89}\text{Zirconium}$ for Positron Emission Tomography (PET) Imaging. *Chempluschem* **2016**, *81*, 274–281. [[CrossRef](#)] [[PubMed](#)]
20. Buchwalder, C.; Rodriguez-Rodriguez, C.; Schaffer, P.; Karagiozov, S.K.; Saatchi, K.; Hafeli, U.O. A new tetrapodal 3-hydroxy-4-pyridinone ligand for complexation of $^{89}\text{Zirconium}$ for positron emission tomography (PET) imaging. *Dalton Trans.* **2017**, *46*, 9654–9663. [[CrossRef](#)] [[PubMed](#)]
21. Adams, C.J.; Wilson, J.J.; Boros, E. Multifunctional Desferrichrome Analogues as Versatile $^{89}\text{Zr(IV)}$ Chelators for ImmunoPET Probe Development. *Mol. Pharm.* **2017**, *14*, 2831–2842. [[CrossRef](#)] [[PubMed](#)]
22. Pandya, D.N.; Bhatt, N.; Yuan, H.; Day, C.S.; Ehrmann, B.M.; Wright, M.; Bierbach, U.; Wadas, T.J. Zirconium tetraazamacrocycle complexes display extraordinary stability and provide a new strategy for zirconium-89-based radiopharmaceutical development. *Chem. Sci.* **2017**, *8*, 2309–2314. [[CrossRef](#)] [[PubMed](#)]
23. Zhai, C.; Summer, D.; Rangger, C.; Franssen, G.; Laverman, P.; Haas, H.; Petrik, M.; Haubner, R.; Decristoforo, C. Novel bifunctional cyclic chelator for ^{89}Zr labeling–radiolabeling and targeting properties of RGD conjugates. *Mol. Pharm.* **2015**, *12*, 2142–2150. [[CrossRef](#)] [[PubMed](#)]
24. Summer, D.; Rangger, C.; Klingler, M.; Laverman, P.; Franssen, G.M.; Lechner, B.E.; Orasch, T.; Haas, H.; von Guggenberg, E.; Decristoforo, C. Exploiting the Concept of Multivalency with ^{68}Ga - and ^{89}Zr -Labelled Fusarinine C-Minigastrin Bioconjugates for Targeting CCK2R Expression. *Contrast Media Mol. Imaging* **2018**, *2018*, 3171794. [[CrossRef](#)] [[PubMed](#)]
25. Summer, D.; Garousi, J.; Oroujeni, M.; Mitran, B.; Andersson, K.G.; Vorobyeva, A.; Lofblom, J.; Orlova, A.; Tolmachev, V.; Decristoforo, C. Cyclic versus Noncyclic Chelating Scaffold for ^{89}Zr -Labeled ZEGFR:2377 Affibody Bioconjugates Targeting Epidermal Growth Factor Receptor Overexpression. *Mol. Pharm.* **2018**, *15*, 175–185. [[CrossRef](#)] [[PubMed](#)]
26. Vosjan, M.J.; Perk, L.R.; Visser, G.W.; Budde, M.; Jurek, P.; Kiefer, G.E.; van Dongen, G.A. Conjugation and radiolabeling of monoclonal antibodies with zirconium-89 for PET imaging using the bifunctional chelate p-isothiocyanatobenzyl-desferrioxamine. *Nat. Protoc.* **2010**, *5*, 739–743. [[CrossRef](#)] [[PubMed](#)]
27. Petrik, M.; Zhai, C.; Novy, Z.; Urbanek, L.; Haas, H.; Decristoforo, C. In vitro and in vivo comparison of selected Ga-68 and Zr-89 labelled siderophores. *Mol. Imaging Biol.* **2016**, *18*, 344–352. [[CrossRef](#)] [[PubMed](#)]

